Solution Structure of Loop A from the Hairpin Ribozyme from Tobacco Ringspot Virus Satellite†

Zhuoping Cai and Ignacio Tinoco, Jr.*

Department of Chemistry, University of California at Berkeley, and Structural Biology Division, Lawrence Berkeley National Laboratory, Berkeley, California 94720

Received December 18, 1995; Revised Manuscript Received March 18, 1996⊗

ABSTRACT: The solution structure of loop A from the hairpin ribozyme found in the minus strand of tobacco ringspot virus satellite has been determined by NMR spectroscopy. The ribozyme consists of two internal loops flanked by short helices: loop A and helices I and II include the substrate and substrate binding site; loop B and helices III and IV are the catalytic domain. Loop A is a symmetric internal loop of eight nucleotides that contains the cleavage site. The 2-amino group of the guanine immediately 3′ to the cleavage site is essential for catalysis. NMR results show that this guanine forms a sheared G·A base pair. The cytosine residue immediately 5′ to the cleavage site forms an AH^+·C base pair with an adenine whose pK_a is shifted to 6.2 to allow partial protonation near neutral pH. Although the residues flanking the cleavage site are stacked in an A-form pattern, the phosphodiester backbone next to the cleavage site on the 3′ side is splayed apart. This places the following base—a uracil—in the expanded major groove. The conformational flexibility and the lack of steric hindrance of the uracil as well as the unoccupied Watson−Crick positions on the sheared G·A base pair can allow loop A to specifically interact with the catalytic domain (loop B) without drastically changing its own conformation. The three-dimensional structure of loop A provides explanations for previously published mutation and structural mapping results.

Structural information about RNA loops (hairpin loops, internal loops, and bulge loops) is important for understanding mechanisms and functions of RNA. Structural studies on RNA loops have shown that non-Watson−Crick base-paired nucleotides can form unique three-dimensional conformations through formation of mismatched base pairs, base−backbone and base−sugar interactions, and base−base and base−sugar stacking [for reviews, see Shen et al. (1995) and Wyatt and Tinoco (1993)]. The internal loop is a double-stranded region of RNA that has nucleotides not involved in Watson−Crick base pairs on both strands. This type of loop is associated with important functions of RNA, including RNA−protein binding, RNA−RNA interactions, and RNA catalysis (Wyatt & Tinoco, 1993; Pan & Uhlenbeck, 1992; Hampel & Tritz, 1989).

Two internal loops (loop A and loop B) and their flanking helices (helices I, II, III, and IV) shown in Figure 1A constitute the catalytic core of a hairpin ribozyme derived from the minus strand of tobacco ringspot virus satellite RNA (Hampel & Tritz, 1989). The catalytic core consists of a 50-nucleotide ribozyme strand and a 14-nucleotide substrate strand. The ribozyme catalyzes a site-specific reversible cleavage reaction which generates products with 5′-hydroxyl and 2′,3′-cyclic phosphate termini (Buzayan et al., 1986). Most of the essential nucleotides for catalysis are found in the two loops (Anderson et al., 1994; Berzal-Herranz et al., 1993). The catalytic function makes the hairpin ribozyme a potentially useful therapeutic agent, and the ribozyme has been engineered to specifically cleave the HIV-1 RNA (Yu et al., 1995; Joseph & Burke, 1993; Ojwang et al., 1992).

While a wealth of information about the sequence requirement, catalytic function, and structural characteristics of the hairpin ribozyme has been accumulated through mutagenesis, *in vitro* selection, chemical modification, photo-cross-linking, and other studies, the three-dimensional structure of the ribozyme remains unknown [for a review, see Burke (1994)]. Detailed knowledge of the hairpin ribozyme structure will be valuable for understanding and improving its catalytic activitiy. The 64-nucleotide ribozyme−substrate complex is small compared to other biologically important RNA molecules. However, it is considered large for determining detailed three-dimensional conformation using NMR.[1] Our goal is to first determine the individual structures of loop A and loop B. Structural information obtained from the individual internal loops will not only add to our limited knowledge of RNA loop structures but also greatly facilitate solving the conformation of the entire hairpin ribozyme−substrate complex. In this study, we used NMR spectroscopy followed by structural calculations using restrained molecular dynamics to determine the conformation of the loop A domain, which includes loop A, helix I, and helix II (Figure 1B). Loop A is a symmetrical internal loop of eight nucleotides that contains the cleavage site.

† This research was supported in part by National Institutes of Health Grant GM 10840, by Department of Energy Grant DE-FG03-86ER60406, and through instrumentation grants from the Department of Energy (DE-FG05-86ER75281) and from the National Science Foundation (DMB 86-09305).

* To whom correspondence should be addressed.

⊗ Abstract published in *Advance ACS Abstracts,* May 1, 1996.

[1] Abbreviations: NMR, nuclear magnetic resonance; NOE, nuclear Overhauser effect; NOESY, NOE spectroscopy; DQF-COSY, double-quantum-filtered, correlation spectroscopy; HMQC, heteronuclear multiple-quantum correlation spectroscopy; rMD, restrained molecular dynamics; FID, free induction decay; 1D, one dimensional; 2D, two dimensional; rmsd, root mean square deviation; EDTA, ethylenediaminetetraacetic acid; TSP, 3-(trimethylsilyl)propionate; TMP, trimethyl phosphate; NiCR, (2,12-dimethyl-3,7,11,17-tetraazabicyclo[11.3.1]-heptadeca-1(17),2,11,13,15-pentaenato) nickel(II) perchlorate.

S0006-2960(95)02985-0 CCC: $12.00

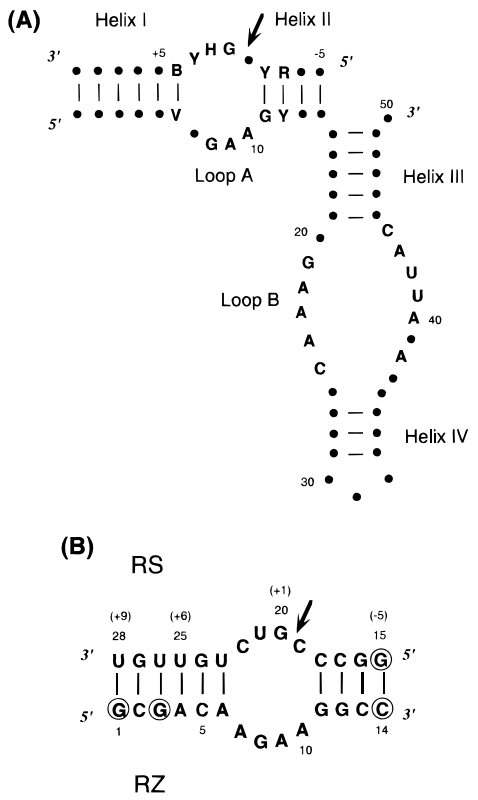

FIGURE 1: (A) Essential primary and secondary structure of the catalytic core of the hairpin ribozyme−substrate complex (Berzal-Herranz et al., 1993). Arrow indicates cleavage site. Ribozyme nucleotides are numbered from 1 to 50 in the catalytic core region. Substrate nucleotides are numbered consecutively from the cleavage site: negative for those to the 5′ side of the cleavage site; positive for those to the 3′ side. Dots indicate any base; B indicates C, G, or U; H indicates A, C, or U; R indicates G or A; V indicates A, C, or G; and Y indicates C or U. (B) Sequence of the loop A domain used in this study. The sequence was adapted from the hairpin ribozyme designed to cleave HIV-1 RNA [see Ojwang et al. (1992)]. The circled nucleotides were modified to facilitate transcription using T7 polymerase. RZ is the ribozyme strand and RS is the substrate strand. In this study, RZ is numbered from 1 to 14; RS is numbered from 15 to 28. Numbers in parentheses indicate the more commonly used numbering scheme for the substrate.

MATERIALS AND METHODS

RNA Synthesis and Purification. The two strands of the loop A domain, 5′-pppGCGACAAGAAGGCC (RZ) and 5′-pppGGCCCGUCUGUUGU (RS), were enzymatically synthesized using T7 polymerase from synthetic DNA templates (Wyatt et al., 1991; Milligan et al., 1987). Crude RNAs were purified using denaturing polyacrylamide gel electrophoresis. The yields of RNA were 50−70 nmol of RNA/mL of reaction for RZ and 35−52 nmol/mL of reaction for RS. The $n - 1$ product of RS, which had significantly higher yield (60−80 nmol/mL of reaction) than the full-length RS, was also used in some NMR experiments. Except for the terminal two base pairs of helix I, NMR spectra obtained from samples with RS($n - 1$) were virtually identical to those obtained with the full-length RS. The RNA sequences were verified by enzymatic digestion using RNases A, T1, U2, and CL3.

Selective ^{13}C-Labeling of RNA. Selectively ^{13}C-labeled nucleotide monophosphates (NMPs) were chemically synthesized by Dr. John SantaLucia (SantaLucia et al., 1995) and enzymatically phosphorylated to nucleotide triphosphates (NTPs) (Hines et al., 1994). The pyrimidines and purines were ^{13}C-labeled at C6 and C8 positions, respectively. RNA oligonucleotides were synthesized enzymatically with labeled NTPs at an optimized Mg^{2+} concentration.

Uniform ^{13}C/^{15}N-Labeling of RNA. NMPs uniformly ^{13}C/^{15}N-labeled at 99% enrichment were isolated from *Methylophilus methylotrophus* bacterial cells and enzymatically phosphorylated to NTPs (Hines et al., 1994). RNA oligonucleotides were synthesized enzymatically with labeled NTPs at an optimized Mg^{2+} concentration.

NMR Spectroscopy. RNA samples used in NMR studies were dialyzed extensively (∼48 h) against 2 × 2 L of buffer. The buffer used in most NMR experiments contained 150 mM NaCl, 10 mM sodium phosphate, and 10 μM EDTA (pH 6.4). Samples used for exchangeable proton experiments were lyophilized and resuspended in 90% H_2O/10% D_2O. Samples for nonexchangeable proton experiments were lyophilized twice from D_2O and then resuspended in 99.96% D_2O (Aldrich). Sample concentrations were 1.8−2.7 mM. Both proton and carbon chemical shifts were referenced to an internal TSP standard at 0.00 ppm; phosphorus chemical shifts were referenced to an external TMP standard at 0.00 ppm; and nitrogen chemical shifts were indirectly referenced to liquid NH_3 at 0.00 ppm (Live et al., 1984).

One-dimensional (1D) exchangeable proton spectra were taken on GE GN-500 using a 1-1 sequence for solvent suppression (Plateau & Guéron, 1982). The first excitation maximum was set between the imino and aromatic regions so that the second excitation maximum was at the center of the imino region. A total of 4096 complex points were collected with 256 scans and a sweep width of 12500 Hz.

All two-dimensional (2D) NMR experiments were done on a GE GN-500 or Bruker AMX-600 spectrometer, except for the heteronuclear correlated ^{1}H−^{31}P experiment which was done on a Bruker AMX-300. All NMR data were processed using FELIX (Biosym Technologies, Inc.). All NMR experiments in D_2O were done at 22 °C unless otherwise mentioned.

NOESY spectra in H_2O were taken at 5, 15, and 22 °C using a 1-1 sequence for solvent suppression. The first maximum of excitation was set either on the aromatic region to enhance the imino-to-imino NOEs or between the imino and aromatic regions. The carrier frequency and the second 90° pulse were optimized for better solvent suppression. Approximately 370 FIDs of 1024 complex points and 80 scans were collected with a relaxation delay of 2.0 s and mixing times of 120 and 300 ms. The sweep width was 12 000 Hz in both dimensions.

NOESY spectra in D_2O were taken at 17, 22, and 27 °C with a mixing time of 250 ms. For estimating NOE intensities, additional NOESY spectra were taken with mixing times of 50, 100, and 150 ms. Approximately 380 FIDs with 1024 complex points and 80 scans were collected with a relaxation delay of 2.5 s. The sweep width was 5000 Hz in both dimensions.

A high-resolution, phosphorus-decoupled, double-quantum-filtered (DQF) COSY spectrum was taken at 600 MHz. A total of 677 FIDs of 2048 complex points and 32 scans were collected with a sweep width of 2000 Hz in both dimensions. The relaxation time was 2.5 s.

A heteronuclear correlated ^{1}H−^{31}P spectrum was taken at 300 MHz (^{1}H). Sweep widths were 1380 Hz in ω_2 (^{1}H) and 600 Hz in ω_1 (^{31}P), respectively. A total of 211 FIDs of

2048 complex points and 176 scans were collected with a relaxation delay of 2.5 s.

ω_1 $^1/_2$-X-filtered NOESY experiments were done in D_2O on a sample selectively ^{13}C-labeled on the RZ strand (SantaLucia et al., 1995; Otting & Wüthrich, 1990). A composite 180° pulse on ^{13}C was used in ω_1 for $^1H-^{13}C$ decoupling; WALTZ-16 sequence was used for broad-band $^1H-^{13}C$ decoupling in ω_2. The mixing times were 60, 120, and 250 ms. For each t_1 increment, two FIDs were collected, one with and the other without an 180° ^{13}C pulse. The two sets of FIDs were added and subtracted in data processing to produce a ^{12}C subspectrum and a ^{13}C subspectrum, respectively. Approximately 670 FIDs of 1024 complex points and 32 scans were acquired with a relaxation delay of 2.5 s.

A 3D HMQC-NOESY experiment was done in D_2O on a sample selectively ^{13}C-labeled on the RZ strand (SantaLucia et al., 1995). The ^1H carrier was set to 7.5 ppm, except for presaturation during the 2 s relaxation delay and the last 90 °C pulse which was set to ~4.7 ppm. The ^{13}C carrier was set at 140 ppm. The sweep widths were 1500 (ω_1), 1200 (ω_2), and 5000 Hz (ω_3). Real data points acquired for the three dimensions were 32 in ω_1, 64 in ω_2, and 1024 in ω_3. The NOESY mixing time was 250 ms.

A double $^1/_2$-X-filtered NOESY experiment was done in D_2O on a sample with uniformly $^{13}C/^{15}N$-labeled strand RS(n − 1) (Wider et al., 1990). Filters were used such that ^{13}C-bound and ^{12}C-bound protons were selected in ω_1 and ω_2 dimensions, respectively. The mixing time was 250 ms. A total of 290 FIDs of 1024 complex points and 128 scans were collected over a sweep width of 5000 Hz in both dimensions with a relaxation delay of ~0.9 s.

^1H-^{13}C HMQC experiments were done in D_2O at various pHs on a sample with uniformly $^{13}C/^{15}N$-labeled guanosines and adenosines on strand RZ. The pD values were titrated using 10 mM DCl and NaOD and were converted to pH values by adding 0.4 unit to correct for the isotope effect (Primrose, 1993). For the aromatic H2/H8 to C2/C8 region, the ^1H and ^{13}C carriers were set at ~4.8 ppm and ~145 ppm, respectively. The sweep widths were 5000 and 4000 Hz for ^1H (ω_2) and ^{13}C (ω_1), respectively. Approximately 150 FIDs of 512 complex points and 80 scans were collected. The sweep widths were 5000 Hz in ω_2 and 4000 Hz in ω_1.

An $^1H-^{15}N$ HMQC experiment with 1-1 solvent suppression sequence was done in H_2O on a sample with uniformly $^{13}C/^{15}N$-labeled strand RS(n − 1). The first excitation maximum for protons was set at 13 ppm. The ^1H and ^{15}N carriers were set at 4.8 and 150 ppm, respectively. The sweep widths were 13 000 and 1825 Hz for ^1H (ω_2) and ^{15}N (ω_1), respectively. A total of 128 FIDs of 512 complex points were collected with 160 scans.

Interproton Distance and Torsion Angle Constraints. Interproton distances between nonexchangeable protons were estimated by integrating cross-peak intensities in NOESYs at 50, 100, and 150 ms mixing times. The pyrimidine H5−H6 distance (2.41 Å) was used as reference. NOEs were classified as strong, medium, weak, very weak, and for a few unambiguous cases, absent. The corresponding distances were 1.8−3, 2.5−4, 3−5, 3−6.5, and >3.5 Å, respectively. The very weak NOEs were observed clearly above noise level at 250 ms but not at 150 ms. Interproton distances were set to >3.5 Å (absent NOEs) only if the cross peak, if present, would have appeared in a visible area of the NOESY, and the protons have other NOE cross peaks. Lower bounds of distance constraints were loosened for protons that have unusually broad line width due to dynamic motion on the intermediate time scale. Distances obtained from 3D HMQC-NOESY were given looser constraint ranges. When NOEs were observed at 120 ms, interproton distances involving both exchangeable and nonexchangeable protons were assumed to be 3−6 Å and those involving only exchangeable protons were assumed to be 3−5 Å.

Sugar puckers were determined from $J_{1'2'}$ values measured in the high-resolution DQF-COSY. A sugar conformation was constrained to C3′-*endo* if the H1′ to H2′ cross-peak is absent, to C2′-*endo* if $J_{1'2'}$ is ≥10 Hz, and to within a broad range from C2′-*endo* to O4′-*endo* to C3′-*endo* if $J_{1'2'}$ is <10 Hz. The glycosidic angle χ was constrained to be *anti* (−120 ± 90°) for nucleotides that do not have strong intranucleotide H1′−H8 NOEs at short mixing times (50−100 ms).

Structure Calculation. The structure of the loop A domain was calculated using the X-PLOR 3.1 package with restrained molecular dynamics (rMD) (Brünger, 1992). Forty starting structures generated using random torsion angles were calculated by rMD and simulated annealing. To shorten the calculation time, only three base pairs from each stem were included. The protocol for structural calculation included two stages: global fold and refinement. The global fold used rMD at 1000 K; the slope for distance violations above the upper constraint limits and the force constant for the repulsive-only van der Waals potential were gradually increased during rMD. The refinement stage was divided into two steps. The first step used rMD at 1000 K while increasing the force constant for torsion angle potentials. Up to this point, electrostatic potential and the attractive term of the Lennard-Jones potential were not applied. These potentials were on only in the second step of refinement which used rMD at 300 K. All steps of rMD calculation were followed by energy minimization.

RESULTS

Assignment of Nonexchangeable Proton Resonances. The assignments of nonexchangeable proton resonances are shown in Table 1. To overcome the problem of spectral overlap, we selectively ^{13}C-labeled the RZ strand at C6 of pyrimidines and C8 of purines. By using an ω_1 $^1/_2$-X-filtered NOESY experiment, we obtained two subspectra of loop A, one with ^{13}C-bound protons and the other with ^{12}C-bound protons in the ω_1 dimension (Figure 2B,C). In essence, the aromatic−sugar NOE connectivities of the RZ and RS strands were separated into the two subspectra. Compared with the NOESY spectrum of the unlabeled molecule (Figure 2A), the subspectra were greatly simplified, allowing many overlapping peaks to be resolved. For example, the G_8 H1′−H8 cross-peak is completely buried under the U_{28} H5−H6 cross-peak in the regular NOESY, but these peaks were separated in the two subspectra. To further disperse the aromatic−sugar region of the NOESY spectrum, we used a 3D HMQC-NOESY experiment which edits the NOESY spectrum according to ^{13}C chemical shifts in a third dimension.

However, spectral regions involving sugar protons could not be simplified by selective ^{13}C-labeling of C8/C6 positions. To identify cross-strand sugar-to-sugar NOEs, a double $^1/_2$-X-filtered NOESY experiment was done on a

Table 1: Proton Chemical Shifts (ppm) of Loop A Domain[a]

residue	H8/H6	H/H2	H1′	H2′	H3′	H4′	H5′/H5″	imino	amino
G1	8.20	na[b]	5.82	4.87	4.67	4.55	4.54/4.26	11.10	
C2	7.81	5.56	5.73	4.59	4.46			na	
G3	7.57	na	5.75	4.78	4.44			10.26	
A4	7.85	7.80	5.90	4.46	4.68	4.49	4.60/4.15	na	
C5	7.43	5.13	5.36	4.38				na	8.02/6.87
A6	7.71	6.82	5.74	4.34	4.45		4.44/4.08	na	
A7	7.89	7.41	5.58	4.62	4.66	4.47		na	
G8	7.65	na	5.45	4.58	4.82	4.66	4.23		
A9	8.05	7.97	5.61	4.93	4.75	4.45	4.22	na	
A10	8.23	8.17	5.84	4.82	4.76			na	
G11	6.91	8.17	5.84	4.82	4.24		4.33/4.02	12.62	
G12	7.29	na	5.81	4.51			4.55/4.04	13.26	
C13	7.62	5.20	5.54	4.33				na	8.68/6.92
C14	7.69	5.57	5.78	4.03	4.18			na	8.38/7.04
C15	8.16	na	5.81	4.93	4.76	4.56	4.44/4.30	12.94	
G16	7.72	na	5.94	4.57	4.45			13.50	
C17	7.69	5.25	5.55	4.39				na	8.59/6.87
C18	7.63	5.41	5.43	4.53	4.32	4.39		na	8.33/6.81
C19	7.52	5.52	5.50	3.90	4.26	4.75	4.64/4.03	na	
G20	8.09	na	5.57	4.98	4.71			10.40	
U21	7.67	5.70	5.43	4.60	4.58		3.76/3.36		na
C22	8.08	5.85	5.94	4.46	4.68	4.50		na	
U23	7.89	5.71	5.35	4.68	4.42	4.55	4.23	13.40	na
G24	7.81	na	5.82	4.55				12.47	
U25	7.60	5.19	5.49	4.64	4.34	4.45		14.30	na
U26	7.90	5.77	5.52	4.29	4.57			11.73	na
G27	7.87	na	5.74	4.42				13.08	
U28	7.65	5.44	5.72	4.04	4.19			12.06	na

[a] All assignments were made in 150 nM NaCl, and 10 mM sodium phosphate, and 10 μM EDTA (pH 6.4) at 22 °C for nonexchangeable protons and at 5 °C for exchangeable protons. All proton chemical shifts are referenced to TSP. [b] na = not applicable.

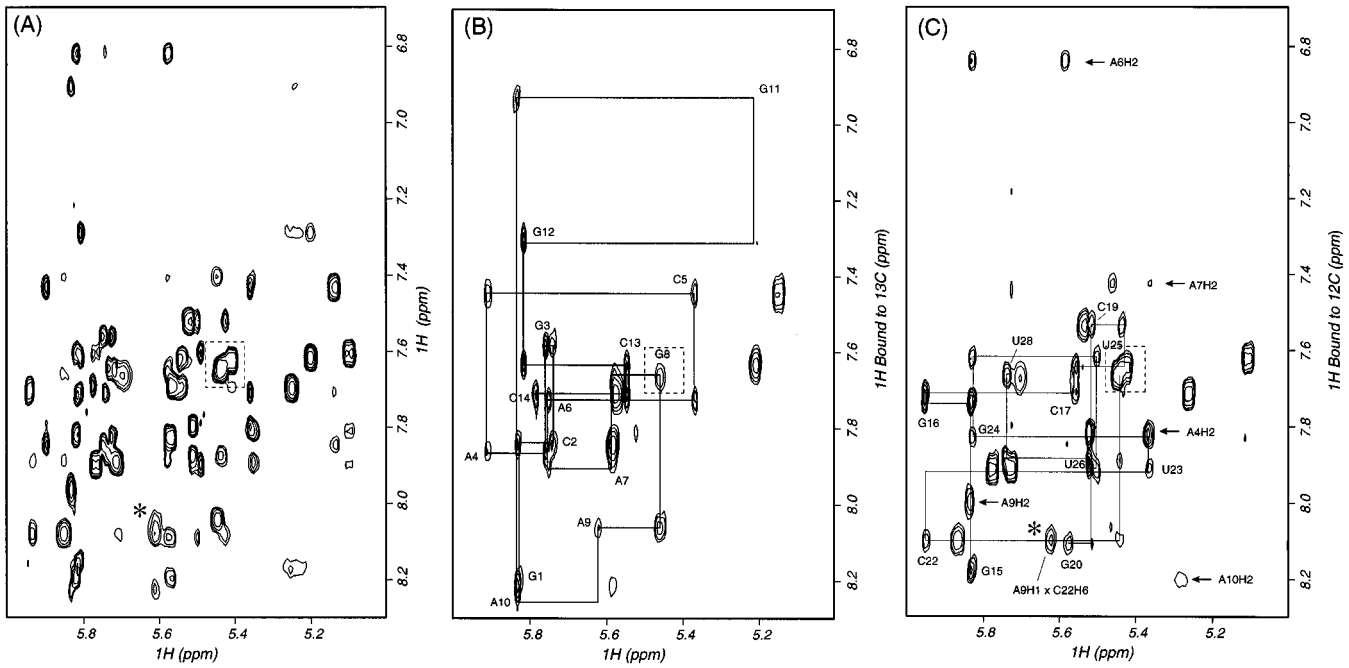

FIGURE 2: Comparison of the NOESY spectrum of the unlabeled loop A domain with $^1/_2$-X-filtered NOESY spectra of the molecule selectively ^{13}C-labeled on the RZ strand. Spectra were taken at 22 °C in 150 mM NaCl, 10 mM sodium phosphate, and 10 mM EDTA (pH 6.4); the mixing time was 250 ms. The H8/H6/H2 to H1′/H5 region of the spectra is shown. (A) NOESY spectrum. (B) ^{13}C subspectrum of $^1/_2$-X-filtered NOESY showing NOE connectivities in the RZ strand. (C) ^{12}C subspectrum of $^1/_2$-X-filtered NOESY showing NOE connectivities in the RS strand. The boxed area in (A) shows a crowded spectral region where the G_8 H8 to H1′ cross-peak is completely buried under the U_{28} H5 to H6 cross-peak in the regular NOESY spectrum but resolved in the $^1/_2$-X-filtered NOESY spectra (C). The asterisk in (C) indicates an unusual cross-peak from C_{22} H6 to A_9 H1′.

sample with only the RS(n − 1) strand uniformly labeled by ^{13}C/^{15}N. By using appropriate filters, we selected NOEs only between ^{13}C-bound and ^{12}C-bound protons. An unusual NOE was found between A_9 H4′ and U_{21} H1′ which was buried in the crowded H1′/H5-sugar region in the regular NOESY spectrum.

The AH2 protons were identified on the basis of the C2 chemical shifts in the ^{1}H−^{13}C HMQC experiment using a uniformly ^{13}C/^{15}N-labeled sample (Varani & Tinoco, 1991). The sequential NOEs from the AH2 protons to the H1′ protons on the 3′ side were used to assign the AH2 resonances. For A_4, A_6, and A_7, assignments of H2 protons

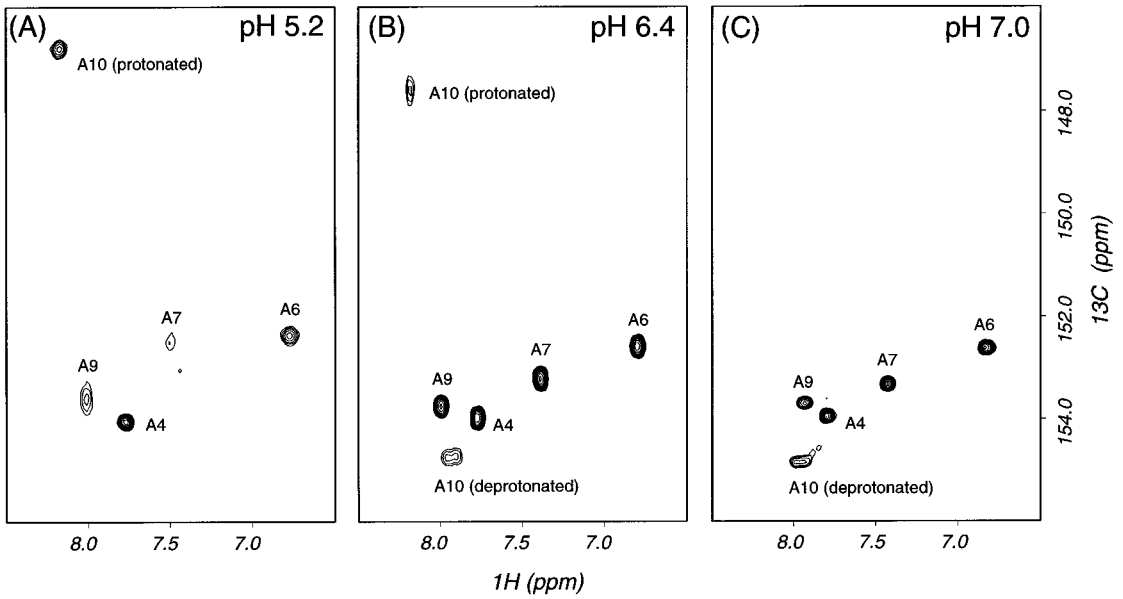

FIGURE 3: Aromatic C2 to H2 region of $^{1}H-^{13}C$ HMQC spectra at (A) pH 5.2, (B) pH 6.4, and (C) pH 7.0. Spectra were taken at 25 °C on a sample uniformly $^{13}C/^{15}N$-labeled at guanosines and adenosines on the RZ strand. The two C2−H2 cross-peaks seen for A_{10} indicate slow exchange between the protonated and unprotonated species.

were also confirmed by their NOEs to the cross-strand H1′ protons on the 3′ side.

Partial Protonation of A_{10} near Neutral pH. The C2 resonance of adenine is upfield shifted by 8 ppm upon protonation at its N1 position (Legault & Pardi, 1994). In loop A the C2 resonance of A_{10} was upfield shifted by 8.0 ppm when pH was decreased from 7.0 to 5.2, indicating protonation of A_{10} at lower pH (Figure 3A,C). Over the pH range from 5.8 to 6.7, the A_{10} C2 resonance was observed at both chemical shifts, corresponding to the protonated and unprotonated species of A_{10}. The H2 resonance of A_{10} was downfield shifed by 0.25 ppm as pH decreased from 7.0 to 5.2; the resonance was also observed at both chemical shifts over the pH range from 5.8 to 6.7. The lack of intermediate chemical shifts for C2 and H2 and the presence of both protonated and unprotonated species of A_{10} show that the two species are in slow conformational exchange at near neutral pH (Figure 3B). An upper limit to the exchange rate is about 120 s^{-1} based on the 8.0 ppm ^{13}C shift at 151 MHz ($\Delta\nu = 1200$ Hz) and about 15 s^{-1} based on the 0.25 ppm ^{1}H shift at 600 MHz ($\Delta\nu = 150$ Hz). Therefore, the upper limit to the exchange rate obtained from NMR is 15 s^{-1}. Assuming that the intensities of the H2−C2 cross-peaks for the protonated and unprotonated A_{10} are proportional to the populations of the two species, we obtain a pK_a of 6.2 ± 0.1 using intensities measured at four intermediate pHs (pH 5.8−6.7). Thus, A_{10} is about 40% protonated at the pH where most NMR spectra were taken (pH 6.4). The protonated A_{10} can form an AH^+·C base pair with the C_{19} on the substrate strand.

Evidence for Formation of the Sheared G_{20}·A_9 Base Pair. All imino protons in the stems were assigned using 2D H_2O NOESY and 1D temperature-dependent imino spectra (Table 1). A relatively sharp imino peak from the loop was found at 10.40 ppm (Figure 4A). The imino proton was clearly observable even at 25 °C, indicating it is highly protected from exchanging with water. However, the imino resonance was too upfield shifted to be involved in a Watson−Crick base pair. To assign this imino resonance, a 2D $^{1}H-^{15}N$ HMQC spectrum was taken on a sample that contained unlabeled RZ and the $^{13}C/^{15}N$ uniformly labeled RS($n-1$) strand (Figure 4B). The lack of U_{28} in the RS($n-1$) strand only affected the resonances of its nearby nucleotides such as the G_{27} imino proton. On the basis of distinct chemical shifts for the imino nitrogens of G and U, the imino proton at 10.40 ppm was unambiguously assigned to G_{20} because it was the only ^{15}N-labeled G residue in the loop.

The chemical shift of G_{20} imino at 10.40 ppm is consistent with the formation of a sheared G_{20}·A base pair (Heus & Pardi, 1991a; Figure 4C). In addition, the G_{20} imino gives a weak NOE to A_9 H8 at long mixing time (300 ms; Figure 4C). This NOE was observed in two samples with and without Mg^{2+}. The cross-strand NOE along with the characteristic G imino resonance indicates a sheared G_{20}·A_9 base pair, which is the only possible base pairing consistent with the NMR results.

^{31}P Spectrum. Chemical shifts of phosphorus resonances are sensitive to the backbone torsion angles α and ζ. In standard A-form helices where α and ζ angles are *gauche*$^+$, the ^{31}P chemical shifts disperse over a 1 ppm range (Gorenstein, 1984). Shown in Figure 5 is the heteronuclear correlated $^{1}H-^{31}P$ spectrum. Except for six resonances, all the other ^{31}P resonances disperse over a narrow range of 0.9 ppm (−3.8 to −4.7 ppm), suggesting α and ζ angles are consistent with the A-form helices. Among the six non-A-form resonances, four are only slightly off from the A-form range, whereas the other two are unusually downfield shifted at around −1.7 ppm (G_8pA_9 and $U_{21}pC_{22}$), suggesting unusual backbone conformation in the loop region. Due to degeneracy of H3′ resonances, not all the unusually shifted phosphorus resonances could be assigned unambiguously. Therefore, none of the loop backbone torsion angles were restrained.

Structural Features Determined by NMR. NOE connectivities, sugar puckers, ^{31}P chemical shifts, and other NMR results reveal a great deal of structural information about the RNA molecule. The schematic structure of the loop A domain determined by NMR is shown in Figure 6. Except

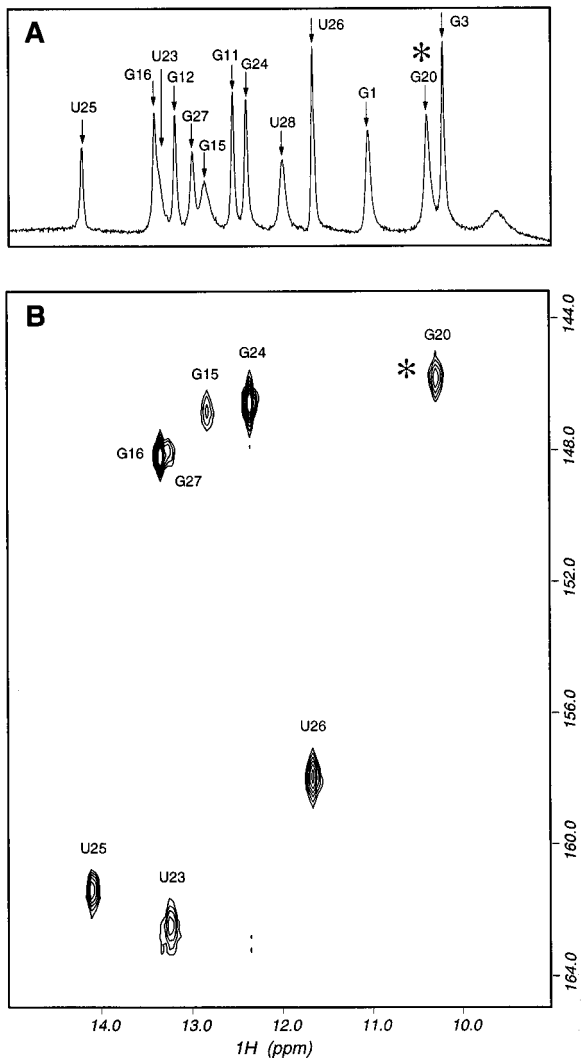

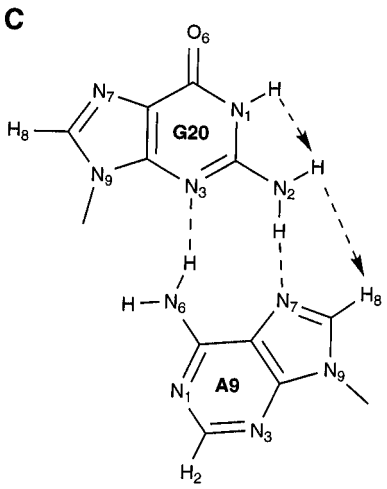

FIGURE 4: Assignment of the G_{20} imino resonance and evidence for the G_{20}·A_9 base pair. All spectra were acquired in 150 mM NaCl, 10 mM sodium phosphate, and 10 mM EDTA (pH 6.4). The G_{20} imino resonance is indicated by an asterisk. (A) 1D imino spectrum of the loop A domain (5 °C). (B) $^1H-^{15}N$ HMQC spectrum on a sample with a uniformly $^{13}C/^{15}N$-labeled RS($n-1$) strand (15 °C). From the distinct ^{15}N resonances of U and G, the loop imino proton resonance at 10.40 ppm was unambiguously assigned to G_{20}. (C) A sheared G·A base pair is consistent with the G_{20} imino resonance and the NOE from G_{20} imino to A_9 H8. Arrows indicate the NOE spin diffusion pathway from G_{20} imino to A_9 H8.

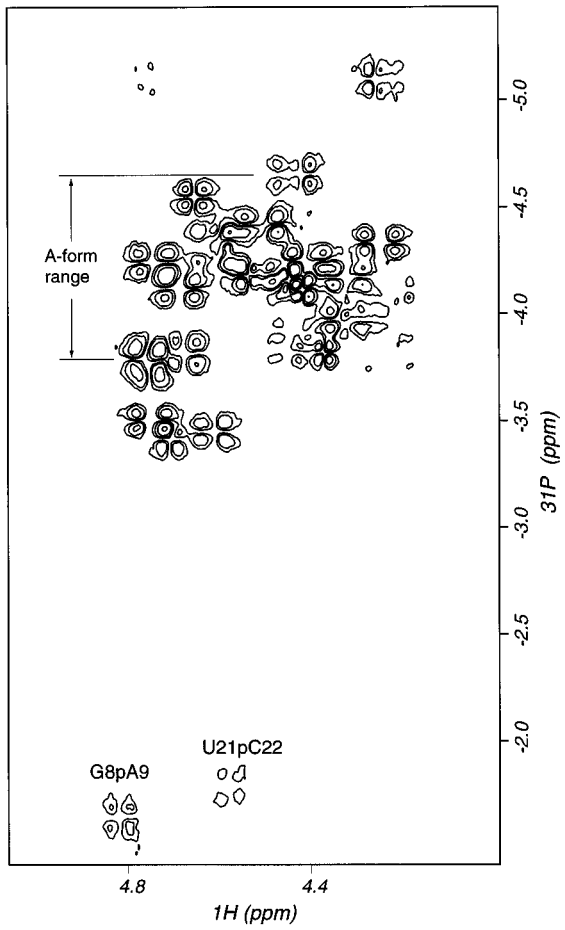

FIGURE 5: Heteronuclear correlated $^1H-^{31}P$ spectrum of the loop A domain in 150 mM NaCl, 10 mM sodium phosphate, and 10 mM EDTA (pH 6.4) at 22 °C. The 0.9 ppm A-form range is indicated. Only the two unusually downfield-shifted phosphorus resonances are labeled.

for the terminal regions, both helix I and helix II have A-form NOE connectivities and C3′-*endo* sugar puckers found in A-like helices. The glycosidic angle χ is *anti* for all the residues. In the loop, three residues (A_9, A_{10}, and C_{19}) have C3′-*endo* sugar puckers, two (G_8 and G_{20}) have C2′-*endo* sugar puckers, and the other three (A_7, U_{21}, and C_{22}) have sugar puckers in between C2′- and C3′-*endo*.

A-form stacking continues from helix II to A_{10} and C_{19}, the loop residues adjacent to the closing base pairs (Figure 6). In addition, the observation of a medium intensity NOE from G_{11} imino to C_{19} H1′ at 120 ms is consistent with the A-form structural feature around the junction between helix II and the loop (Heus & Pardi, 1991b). A_{10} is partially protonated under NMR conditions, which makes it possible to form an $A_{10}H^+$·C_{19} base pair. On strand RZ, A-form stacking extends further to A_9, the second loop residue from helix II; whereas on strand RS, the stacking between C_{19} and G_{20} is only partially A-form, due to the C2′-*endo* sugar pucker of G_{20}. A_9 and G_{20} form a sheared A·G base pair as mentioned earlier.

Whereas the helix II side of loop A (A_9, A_{10}, C_{19}, and G_{20}) is characterized by A-like base stacking and non-canonical base pairing, the helix I side of loop A (A_7, G_8, U_{21}, and C_{22}) displays completely different structural features (Figure 6). In the latter, all four residues have non-C3′-*endo* sugar puckers. Additionally, the unusual NOEs (Table 2) and the two sets of unusual α and ζ angles (Figure 5)

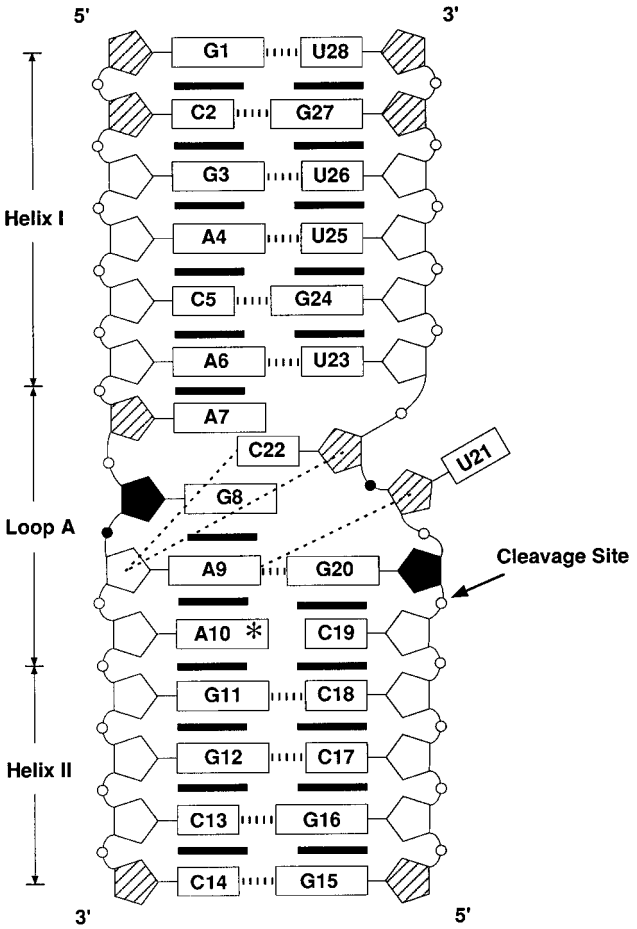

FIGURE 6: Schematic summary of NMR data for the loop A domain. Sugars are represented by pentagons, the patterns of which indicate the sugar puckers: open for C2′-*endo*, solid for C3′-*endo*, and hatched for an equilibrium between C2′- and C3′-*endo*. Phosphate groups are represented by small circles, which are black when the phosphate resonances are unusually downfield shifted. Unusual cross-strand NOEs are indicated by dashed lines. Base stacking is represented by solid bars. Base pairing is represented by hatched bars. The partially protonated adenosine is denoted by an asterisk .

Table 2: Unusual NOEs Observed

NOE observed	intensity	distance constraint (Å)
U21H1′−C22H5	strong	1.8−3.0
A9H1′−C22H6	medium	2.5−4.0
A9H1′−C22H5	very weak	3.0−6.5
A9H1′−C22H1′	very weak	3.0−6.5
A9H4′−C22H1′	medium to strong	1.8−4.0
A9H8−C22H5	very weak	not used
A9H2−U21H4′/5′/5″	very weak	not used

were all found in this part of the loop. On strand RZ, non-A-form stacking was found between G_8 and A_9; on strand RS, a break in NOE connectivity was observed between G_{20} and U_{21}. The two residues are only connected by a very weak NOE from G_{20} H1′ to U_{21} H6; the NOEs from G_{20} H2′ and H3′ to U_{21} H6 are absent. U_{21} is the only pyrimidine in the duplex that has extra broad H5-H6 cross-peaks in NOESY and COSY experiments; other cross-peaks involving U_{21} protons are also broadened. This suggests the residue is in conformational exchange on an intermediate (millisecond) time scale. However, the line-width broadening of U_{21} cannot completely account for the lack of NOE connectivity between G_{20} and U_{21} because intranucleotide sugar-to-base NOEs of U_{21} are clearly present in weak to medium intensities.

C_{22} is connected to A_9 through several unusual NOEs (Table 2). Protons from both the base and sugar of C_{22} have NOEs to the sugar protons of the cross-strand A_9. Except for an unusually strong NOE between C_{22} H5 and U_{21} H1′, C_{22} is connected to U_{21} and U_{23} only by weak NOEs. Thus, C_{22} appears to be closer to strand RZ than to its own RS strand. G_8 and A_7 are connected by weak NOEs, suggesting poor stacking between the two residues. Despite its partial C2′-*endo* sugar pucker, A_7 stacks onto helix I in an A-form pattern.

Structure Calculation. The stems were modeled as canonical A-form helices. Distance constraints in the loop included 100 NOE-based constraints and 8 constraints with an error range of ±0.2 Å to keep the sheared G_{20}·A_9 base pair hydrogen bonded and planar. Backbone torsion angles were not restrained in the loop and the loop−stem junctions.

After the global fold and the first step of refinement using rMD, 10 of the 40 calculated structures were considered converged on the basis of low NOE violations and total energies. The converged structures were then subjected to refinement calculations; both NOE and total energies of all these structures remained low after each refinement step. The precision of the structure was evaluated by calculating the root-mean-square-deviation (rmsd) for all atoms between each converged structure and the calculated average structure. The average of the rmsd values for the five lowest-energy structures was 1.20 Å; the value for the loop and its closing base pairs was also 1.20 Å (Figure 7).

Loop A Structure Is Independent of Mg^{2+}. To determine the effect of magnesium on the structure of the loop A domain, NOESY experiments in both H_2O and D_2O were done on two samples: one with 150 mM NaCl and the other with 3 mM $MgCl_2$ and 60 mM NaCl. Despite minor shifts in resonances, the NOE connectivities from both samples are virtually identical. Magnesium does not appear to have a significant impact on the structure of the loop A domain.

DISCUSSION

Protonation of A_{10} near the Cleavage Site. Although no constraints were used between A_{10} and C_{19}, the two bases in the final structures are coplanar and their relative orientation is close to that in an AH^+·C mismatch (Figure 8). This is consistent with the partial protonation of A_{10} at pH 6.4, the pH at which the NMR constraints were obtained. The pK_a of A_{10} is 6.2, which is significantly higher than that of adenine in the free nucleotide (pK_a = 4.0) and those of the other adenines in the molecule (pK_a < 5.2). Although A_{10} is conserved from mutation studies, C_{19} can be mutated to any other nucleotide without losing catalytic activity (Chowrira et al., 1991). Therefore, the AH^+·C base pair is unlikely to be required for cleavage.

An adenine with high pK_a (pK_a = 6.5) was also found near the cleavage site of a lead-dependent ribozyme (leadzyme) (Legault & Pardi, 1994; Pan & Uhlenbeck, 1992). In the leadzyme, the protonated and unprotonated species of adenine are in rapid exchange, resulting in a single H2−C2 peak whose C2 chemical shift has a sigmoidal dependence on pH (Legault & Pardi, 1994). In the hairpin ribozyme, those species are in slow exchange, resulting in two H2−C2 peaks whose relative intensities rather than chemical shifts

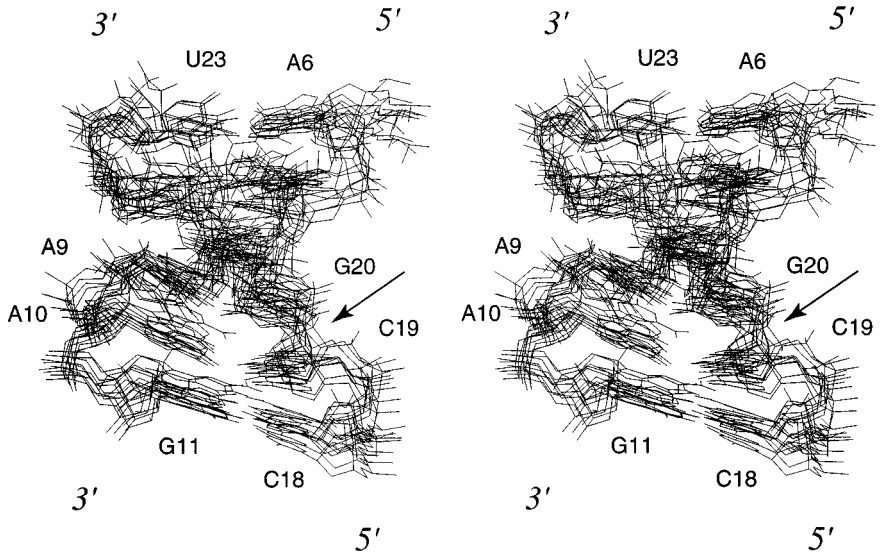

FIGURE 7: Superposition of the ten converged structures of loop A and its closing base pairs. Hydrogen atoms are not shown for clarity. The average of the all-atom rmsd values between the converged structures and the average structure in this region is 1.20 Å.

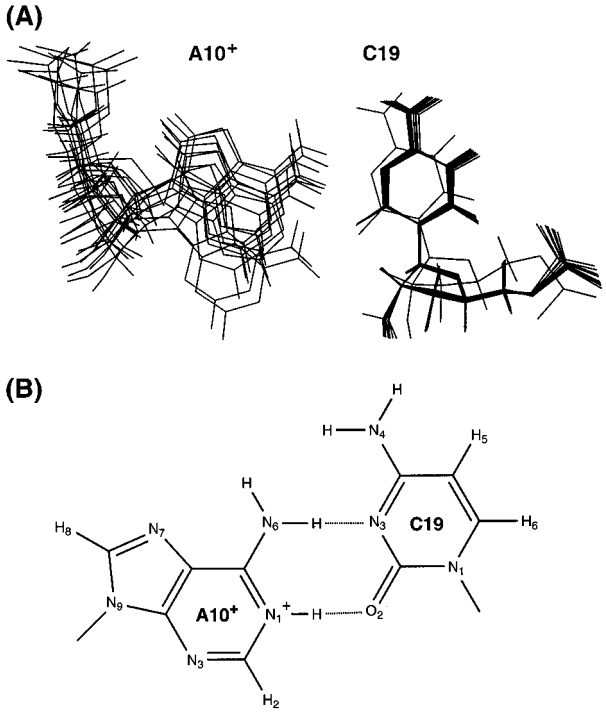

FIGURE 8: (A) Relative orientation of A_{10} and C_{19}. Ten converged structures are superimposed on the basis of C_{19}. No constraints were used between A_{10} and C_{19} in the structural calculation. (B) Proposed $A_{10}H^+ \cdot C_{19}$ base pair.

are pH dependent. The exchange rate of the protonated adenine in the leadzyme ($\geq$1000 s^{-1}) is greater than that in loop A ($\leq$15 s^{-1}) by at least 70-fold. The leadzyme and the hairpin ribozyme are among several ribozymes that share the same catalytic mechanism to generate products with 5′-hydroxyls and 2′,3′-cyclic phosphates. Unlike the hairpin ribozyme which requires two internal loops for its catalytic activity, the cleavage reaction of the leadzyme takes place within a single asymmetric internal loop. At near physiological pH, a partially protonated residue is present near the cleavage site of both the leadzyme and loop A of the hairpin ribozyme, suggesting that protonated residues may play a structural or functional role in RNA catalysis. However, pH dependence studies on the hairpin ribozyme did not seem to support the importance of the protonation of A_{10} (Hampel & Tritz, 1989). The cleavage rate increases by 5-fold as pH increases from 5.5 to 6.5, and it continues to increase from pH 6.5 to 8.0, although with a much samller slope. In fact, the cleavage rate is approximately linearly proportional to the percentage of unprotonated A_{10} from pH 5.5 to 8.0, based on a pK_a of 6.2. The correlation between high cleavage activity and low percentage of protonated A_{10} suggests that protonation of A_{10} inhibits catalysis.

The sequence around the protonated adenine from the loop A in this study is very similar to that from the leadzyme studied by Legault and Pardi (1994). The sequence similarity could be a reason for the similarly high of the adenine in both molecules, although loop A is not catalytically active in the presence of Pb^{2+}.

Conformation at the Cleavage Site. The A-like base stacking at the cleavage site and the splayed phosphodiester linkage 3′ to the cleavage site (G_{20}-U_{21}-C_{22}, Figure 9) bear some similarity to the cleavage site conformation in the crystal structure of the hammerhead ribozyme. In the hammerhead ribozyme, base stacking is also found at the cleavage site although the splayed backbone is 5′ instead of 3′ to the cleavage site. In both molecules, the orientation of the 2′ and 5′ oxygens at the cleavage site is very different from that needed for the in-line attack in the transition state of the cleavage reaction. This is not surprising for loop A, because loop A alone is not catalytically active even in high concentration of magnesium. It was shown that bending of the hairpin ribozyme at the helix II−helix III junction and the critical lengths of helices II and III are required for catalytic activity, suggesting tertiary interactions between loop A and loop B (Komatsu et al., 1994; Feldstein & Bruening, 1993).

Comparison with Mutation and Chemical Modification Data. Mutation data showed that G_{20} (more commonly numbered as G_{+1}), the residue immediately to the 3′ side of cleavage site, is absolutely conserved (Berzal-Herranz et al., 1992). Furthermore, functional group substitution studies indicated that the 2-amino group of G_{20} is required for cleavage (Chowrira et al., 1991). Chowrira et al. proposed that the G_{20} adopts a *syn* conformation which allows its

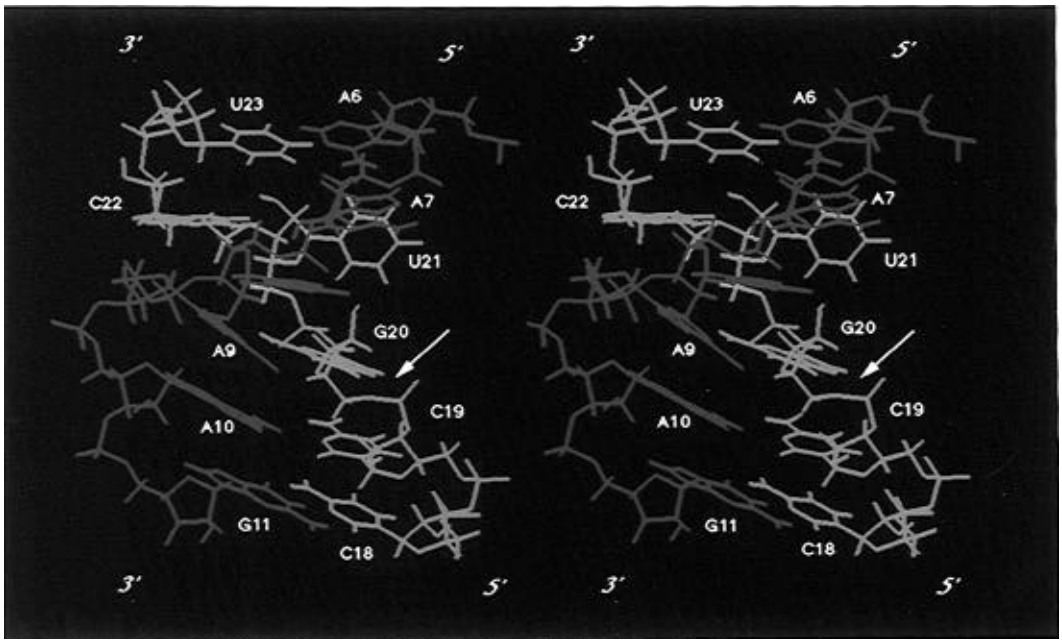

FIGURE 9: Three-dimensional structure of loop A. The loop and closing base pairs of one of the converged structures are shown. Strand RZ is in red and strand RS is in green. The arrow indicates the cleavage site.

2-amino group to lie in close proximity to the scissile P−O bond and the nucleophilic 2′-hydroxyl group immediately 5′ to the cleavage site, which is also required for cleavage. In our NMR-derived structure of the isolated loop A, G_{20} is definitely not in a *syn* conformation. Furthermore, G_{20} and A_9 form a sheared G·A base pair which involves the 2-amino group and N3 of G_{20} and the 6-amino group and N7 of A_9. Functional group substitution results showed that replacing the N7 group of A_9 with C−H ($A_9 \rightarrow N^7$-deaza-A) or deleting the exocyclic 6-amino group of A_9 ($A_9 \rightarrow$ purine ribose) led to substantial drop in k_{cat} whereas K_M was not affected (Grasby et al., 1995). The reduction in binding energy ($\Delta\Delta G_{app}^{\ddagger}$) for these two mutants in the transition state was 2.1 and 1.5 kcal/mol, respectively. These values are sufficient to account for the loss of one or two hydrogen bonds in a G·A base pair (SantaLucia et al., 1992). When the 2-amino group of G_{20} was deleted ($G_{20} \rightarrow$ inosine), however, the reduction in cleavage rate (by 3−5 orders of magnitude) was too great to be accounted for by the loss of hydrogen bonds alone (Grasby et al., 1995; Chowrira et al., 1991). In addition to forming the secondary interactions within loop A, the sheared G_{20}·A_9 base pair could also provide unoccupied Watson−Crick positions for tertiary interactions with loop B.

Another explanation for the essential role of G_{20} in catalysis is that the sheared G_{20}·A_9 base pair in loop A may be required for magnesium binding near the cleavage site. Divalent metal ions such as Mg^{2+} are required for catalysis of the hairpin ribozyme (Chowrira et al., 1993). Grasby et al. (1995) proposed that magnesium binds to the N7 position of G_{20} in the ground state and to the N7 position of A_9 in the transition state. The sheared G·A base pair was also found in conserved sequences of several biologically important RNA molecules, including loop E in *Xenopus* 5S rRNA (Wimberly et al., 1993) and the hammerhead ribozyme (Scott et al., 1995; Pley et al., 1994). The tandem G·A base pairs in the hammerhead ribozyme are not only essential for cleavage activity but also associated with a divalent metal binding site in the crystal structure. However, G·A base pairs and the nearby Mg^{2+} binding site in the hammerhead crystal structure are not close to the cleavage site.

The possible conformations of loop A revealed unusual interactions between G_8 and two cross-strand residues (Figure 10). In eight of the ten final structures, a hydrogen bond forms between the O6 carbonyl group of G_8 and the 2′-hydroxyl proton of G_{20}, with an average distance of 1.80 ± 0.64 Å. In all ten final structures, either the imino or an amino proton of G_8, or both, form hydrogen bonds with the O4′ of U_{21}. Averaged over the ten final structures, the distance between the G_8 imino proton and U_{21} O4′ is 2.04 ± 0.55 Å, and that between the G_8 amino proton and U_{21} O4′ is 2.31 ± 0.40 Å. These cross-strand base-to-sugar hydrogen bonds not only provide additional stabilizing forces in loop A but also explain the chemical modification and mutation results on G_8. Substitution of G_8 with A, U, or C decreased catalytic activity by at least 2 orders of magnitude (Berzal-Herranz et al., 1993). Upon substrate binding, the N1 and N2 positions of G_8 were strongly protected from kethoxal modification; the suppression of reactivity for G_8 was comparable to that for G_6 which forms a Watson−Crick base pair with the substrate. The N7 position of G_8 was also somewhat protected from NiCR upon substrate binding (Butcher & Burke, 1994). However, base−base interactions between G_8 and bases on the substrate strand could not be derived from mutation analysis (Anderson et al., 1994; Joseph et al., 1993). In our structure, the cross-strand hydrogen bonds between the base functional groups of G_8 and the sugar functional groups of the substrate can explain the strong suppression of kethoxal reactivity on G_8 and the lack of base pairing between G_8 and substrate residues.

Although the relatively high precision of the loop A structure adds confidence to the cross-strand hydrogen bond interactions involving G_8, no direct NMR evidence was found to support the formation of these hydrogen bonds. The absence of sharp G_8 imino peak indicated the imino proton of G_8 is not strongly protected from the solvent; however, this does not rule out the possibility for G_8 imino proton to form a hydrogen bond. The amino protons of guanine and

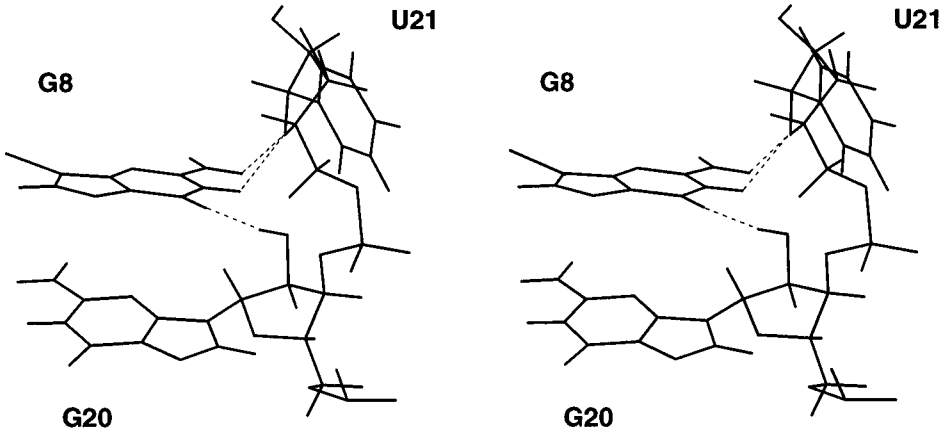

FIGURE 10: Proposed hydrogen bonds found in the converged structures generated by restrained molecular dynamics. Shown here is a stereoview of residues G_8, G_{20}, and U_{21}. Hydrogen bonds between the base of G_8 and the sugars of U_{21} and G_{20} are indicated by dashed lines. In eight of the ten final structures, a hydrogen bond forms between the O6 carbonyl group of G_8 and the 2′-hydroxyl proton of G_{20}. In nine of the ten structures, either the imino proton or an amino proton of G_8 or both form a hydrogen bond with the O4′ of U_{21}.

2′-hydroxyl protons are usually not observable due to rapid chemical exchange.

Comparison with Psoralen Cross-Linking Results. Psoralen cross-linking data revealed several tertiary interactions between U_{21} (or U_{+2}) of the substrate and ribozyme residues in loop B (Monforte, 1991). In our structure of loop A, the substrate residues immediately 5′ and 3′ to U_{21} (G_{20} and C_{22}) are splayed apart, leaving the U_{21} in the widely opened major groove without interacting with other residues in the loop. NMR data also indicated that U_{21} is in dynamic conformational exchange on an intermediate (millisecond) time scale. Besides A_{10}, which is partially protonated, U_{21} is the only other residue in loop A that displays relatively slow dynamic motion. The conformational flexibility and the lack of steric hindrance of U_{21} will allow the residue to form tertiary interactions with loop B without inducing significant conformational changes in loop A.

Structural Implication of Loop A. Although the three-dimensional structure of loop A does not give evidence for the in-line attack involved in the catalysis of the hairpin ribozyme, it allows us to gain insight into how the residues around the cleavage site may interact with the catalytic domain, loop B. The structure demonstrates that non-Watson−Crick base pairing and base−sugar interactions can serve as stabilizing forces in the loop region; these interactions are critical in defining a specific and yet flexible loop A conformation that can be recognized by loop B. The stretched out phosphodiester linkage next to the cleavage site could be another structural feature recognized by loop B. In addition, the stretch widens the major groove and thus could facilitate divalent metal ions to gain entry into the cleavage site. The stretched backbone, which is found near the cleavage site in both loop A and the hammerhead ribozyme, could play an important role in ribozyme catalysis. The three-dimensional structure of the hairpin ribozyme−substrate complex remains to be solved in order to further understand the essential sequence requirement and catalytic function of the hairpin ribozyme. The detailed structure of loop A can help us solve the structure of the ribozyme−substrate complex; it will also allow us to understand how the structure of loop A changes upon addition of loop B.

ACKNOWLEDGMENT

We thank Ms. Barbara Dengler for effectively managing the laboratory and Mr. David Koh for synthesizing the DNA templates used in RNA synthesis and for help to isolate the uniformly $^{13}C/^{15}N$-labeled RNA. We are indebted to Dr. John SantaLucia for synthesizing the selectively ^{13}C-labeled NTPs and the Stable Isotope Resource at Los Alamos National Laboratory for providing cells used in isolation of the uniformly $^{13}C/^{15}N$-labeled NTPs. We also thank Prof. John Burke and Mr. Samuel Butcher at the University of Vermont for sharing their results prior to publication.

REFERENCES

Anderson, P., Monforte, J., Tritz, R., Nesbitt, S., Hearst, J., & Hampel, A. (1994) *Nucleic Acids Res. 22*, 1096−1100.
Berzal-Herranz, A., Joseph, S., Chowrira, B. M., Butcher, S. E., & Burke, J. M. (1993) *EMBO J. 12*, 2567−2574.
Brünger, A. (1992) *X-PLOR Version 3.1. System for X-ray Crystallography and NMR*, Yale University Press, New Haven, CT.
Burke, J. M. (1994) *Nucleic Acids Mol. Biol. 8*, 105−118.
Butcher, S. E., & Burke, J. M. (1994) *J. Mol. Biol. 244*, 52−63.
Buzayan, J. M., Gerlach, W. L., Bruening, G., Keese, P., & Gould, A. R. (1986) *Virology 151*, 186−199.
Chowrira, B. M., & Burke, J. M. (1991) *Biochemistry 30*, 8518−8522.
Chowrira, B. M., Berzal-Herranz, A., & Burke, J. M. (1991) *Nature 354*, 320−322.
Chowrira, B. M., Berzal-Herranz, A., & Burke, J. M. (1993) *Biochemistry 32*, 1088−1095.
Feldstein, P. A., & Bruening, G. (1993) *Nucleic Acids Res. 21*, 1991−1998.
Gorenstein, D. G. (1984) *Phosphorus-31 NMR: Principles and Applications* (Gorenstein, D. G., Ed.) pp 265−296, Academic Press, New York, NY.
Grasby, J. A., Mersmann, K., Singh, M., & Gait, M. J. (1995) *Biochemistry 34*, 4068−4076.
Hampel, A., & Tritz, R. (1989) *Biochemistry 28*, 4929−4933.
Heus, H. A., & Pardi, A. (1991a) *Science 253*, 191−194.
Heus, H. A., & Pardi, A. (1991b) *J. Am. Chem. Soc. 113*, 4360−4361.
Hines, J. V., Landry, S. M., Varani, G., & Tinoco, I., Jr. (1994) *J. Am. Chem. Soc. 116*, 5823−5831.
Joseph, S., & Burke, J. M. (1993) *J. Biol. Chem. 268*, 24515−24518.
Joseph, S., Berzal-Herranz, A., Chowrira, B. M., Butcher, S. E., & Burke, J. M. (1993) *Genes Dev. 7*, 130−138.
Komatsu, Y., Koizumi, M., Nakamura, H., & Ohtsuka, E. (1994) *J. Am. Chem. Soc. 116*, 3692−3696.

Legault, P., & Pardi, A. (1994) *J. Am. Chem. Soc. 116*, 8390−8391.
Live, D. H., Davis, D. G., Agosta, W. C., & Cowburn D. (1984) *J. Am. Chem. Soc. 106*, 1939−1941.
Monforte, J. A. (1991) Ph.D. Thesis, University of California at Berkeley.
Mulligan, J. F., Groebe, D. R., Witherell, G. W., & Uhlenbeck, O. C. (1987) *Nucleic Acids Res. 15*, 8783−8798.
Ojwang, J. O., Hampel, A., Looney, D. J., & Wong-Staal, F. (1992) *Proc. Natl. Acad. Sci. U.S.A. 89*, 10802−10806.
Otting, G., & Wüthrich, K. (1990) *Q. Rev. Biophys. 23*, 39−96.
Pan, T., & Uhlenbeck, O. C. (1992) *Nature 358*, 560−563.
Plateau, P., & Guéron, M. (1982) *J. Am. Chem. Soc. 104*, 7310−7311.
Pley, H. W., Flaherty, K. M., & McKay, D. B. (1994) *Nature 372*, 68−74.
Primrose, W. U. (1993) in *NMR of Macromolecules: A Practical Approach* (Roberts, G. C. K., Ed.) pp 22−23, Oxford University Press, New York, NY.
SantaLucia, J., Jr., Kierzek, R., & Turner, D. H. (1992) *Science 256*, 217−219.
SantaLucia, J., Jr., Shen, L. X., Cai, Z., Lewis, H. A., & Tinoco, I., Jr. (1995) *Nucleic Acids Res. 23*, 4913−4921.
Scott, W. G., Finch, J. T., & Klug, A. (1995) *Cell 81*, 991−1002.
Shen, L. X., Cai, Z., & Tinoco, I., Jr. (1995) *FASEB J. 9*, 1023−1033.
Varani, G., & Tinoco, I., Jr. (1991) *J. Am. Chem. Soc. 113*, 9349−9354.
Wider, G., Weber, C., Traber, R., Widmer, H., & Wüthrich, K. (1990) *J. Am. Chem. Soc. 112*, 9015−9016.
Wyatt, J. R., & Tinoco, I., Jr. (1993) in *The RNA World* (Gesteland, R. F., & Atkins, J. F., Ed.) pp 465−496, Cold Spring Harbor Laboratory Press, Cold Spring Harbor, NY.
Wyatt, J. R., Chastain, M., & Puglisi, J. D. (1991) *BioTechniques 11*, 764−769.
Yu, M., Poeschla, E., Yamada, O., Degrandis, P., Leavitt, M. C., Heusch, M., Yees, J. K., Wong-Staal, F., & Hampel, A. (1995) *Virology 206*, 381−386.

BI952985G